



OPEN ACCESS

EDITED BY

Kavitha Yaddanapudi,
University of Louisville, United States

REVIEWED BY

Jiulong Zhao,
Naval Medical University, China
Yupeng Wang,
Southern Medical University, China

*CORRESPONDENCE

Bo Zhang,
✉ 15821992397@163.com
Wei Wu,
✉ syxx074529@126.com

†These authors have contributed equally
to this work

RECEIVED 24 September 2023

ACCEPTED 16 November 2023

PUBLISHED 29 November 2023

CITATION

Zhang M, Huang Q, Zhang B and Wu W
(2023), Synthesis of organic
photothermal agents for combined
photothermal/enzymatic dynamic
therapy of breast cancer.
Front. Mater. 10:1301177.
doi: 10.3389/fmats.2023.1301177

COPYRIGHT

© 2023 Zhang, Huang, Zhang and Wu.
This is an open-access article distributed
under the terms of the [Creative
Commons Attribution License \(CC BY\)](#).
The use, distribution or reproduction in
other forums is permitted, provided the
original author(s) and the copyright
owner(s) are credited and that the original
publication in this journal is cited, in
accordance with accepted academic
practice. No use, distribution or
reproduction is permitted which does not
comply with these terms.

Synthesis of organic photothermal agents for combined photothermal/enzymatic dynamic therapy of breast cancer

Meifeng Zhang^{1†}, Qian Huang^{2†}, Bo Zhang^{3*} and Wei Wu^{1*}

¹Department of Thyroid and Breast Surgery, Chongming Hospital, Shanghai University of Medicine and Health Sciences, Shanghai, China, ²Department of Oncology, Chongming Hospital, Shanghai University of Medicine and Health Sciences, Shanghai, China, ³Department of General Surgery, Chongming Hospital, Shanghai University of Medicine and Health Sciences, Shanghai, China

Nanoparticle-based photothermal therapy is an effective treatment for superficial tumors. However, due to the highly heterogeneous nature of breast cancer, photothermal therapy (PTT) used alone was unable to achieve satisfactory therapeutic results. Therefore, combining PTT with other therapies is a promising strategy for tumor treatment. Inspired by the significant elevation of lactate levels at the tumor site, we prepared a novel nanocomposite therapeutic platform (PPy-LOX) for combined PTT and enzyme dynamic treatment (EDT) of breast cancer. In detail, Polypyrrole (PPy) nanoparticles were synthesized using a simple chemical oxygenation method and polyvinylpyrrolidone (PVP) was used as a surface linker to enhance its colloidal stability. Further, the loading of lactate oxidase (LOX) is accomplished by simple physical mixing. The *in vivo* and *in vitro* results demonstrated the excellent biocompatibility of the synthesized PPy-LOX NPs. More importantly, PPy-LOX NPs has excellent photothermal conversion ($\eta = 29.9\%$) and lactic acid catalytic ability. On the one hand, the temperature increase induced by near-infrared light irradiation can cause apoptosis of tumor cells; on the other hand, LOX can catalyze the generation of hydrogen peroxide from excess lactate in the tumor microenvironment to induce oxidative stress to kill tumor cells. In conclusion, the combination of PTT and EDT can effectively kill tumor cells. This work provides new ideas on how to design rational nanotherapeutic systems by exploiting the tumor microenvironment.

KEYWORDS

breast cancer, photothermal treatment, polypyrrole, enzyme dynamic therapy, tumor microenvironment

1 Introduction

Based on the latest Global Cancer Burden Report released by GLOBOCAN, breast cancer has become the leading cancer in the world (Siegel et al., 2023). Breast cancer is a highly heterogeneous tumor that poses a serious threat to the health of females (Barzaman et al., 2020). Despite significant advances in the treatment of breast cancer in recent years, the prognosis of breast cancer is still unsatisfactory (Li et al., 2022; Hong and Xu, 2022). Dilemmas in breast cancer treatment include the physical and psychological trauma of surgical removal, resistance to targeted drugs, and the side effects of radiation therapy (Jia et al., 2017; Garcia-Martinez et al., 2021). Therefore, a novel therapeutic strategy with less trauma, fewer side effects, and collegiate treatment is urgently required for the treatment of breast cancer.

In recent years, the rapid development of nanotechnology has brought hope in overcoming tumors (Zhang et al., 2019). A variety of novel therapies such as photothermal therapy (PTT), photodynamic therapy (PDT), chemodynamic therapy (CDT) and enzyme dynamic therapy (EDT) have been developed for the treatment of tumors (Li et al., 2019; Fu et al., 2021; Chang et al., 2022). Notably, breast cancer is highly heterogeneous, and single therapies often fail to achieve complete tumor elimination (Davodabadi et al., 2022). Combining multiple therapies in synergistic fashion may be the best strategy for treating breast cancer.

PTT is a therapeutic method that uses photothermal effect to eliminate tumor cells (Soltero-Rivera et al., 2023). It involves injecting a photothermal conversion material into the body and then using a laser to irradiate the tumor site, causing the material to absorb light energy and convert it into heat energy (Alamdari et al., 2022). The therapeutic efficacy of PTT depends greatly on the performance of the chosen photothermal converter (Zuo et al., 2022). Due to the widespread potential toxicity issues of inorganic photothermal conversion agents, researchers have turned their attention to organic photothermal conversion agents with better biocompatibility (de Melo-Diogo et al., 2017). Polypyrrole (PPy) is a polymer material with excellent electrical conductivity and photothermal conversion properties. Due to these properties, PPy has a wide range of applications in fields such as solar cells, biosensors, and drug carriers (Kumar et al., 2022). It is worth noting that PPy is also used for PTT of tumors due to its excellent photothermal conversion properties (Wu et al., 2021). However, nanomaterials for *in vivo* therapeutic use should have good stability (Dong et al., 2019). Therefore, surface modification of nanomaterials is a prerequisite for their *in vivo* application (Thomsen and Klok, 2021). PVP can form complexes with many other molecules due to its good biocompatibility, solubility and stability (He et al., 2023), which makes it very useful in the preparation of pharmaceutical formulations such as tablets, capsules, emulsions and eye drops (Wei et al., 2023).

Recent studies have shown that due to the heterogeneity of breast cancer, satisfactory treatment results are often not achieved with single therapies (Liang et al., 2020). Currently, combining PTT with other therapies for the treatment of tumors shows great advantages (Huang et al., 2021). Among a variety of kinetic therapies, EDT has attracted much attention as a new type of kinetic therapy. EDT refers to the use of natural enzymes or nano-enzymes with enzyme-catalytic activity to catalyze the conversion of substances in the tumor microenvironment (TME) into highly toxic reactive oxygen species (ROS), thereby killing tumor cells. lactate oxidase (LOX) is an enzyme that can catalyze the oxidation of lactic acid to pyruvate and hydrogen peroxide (Jiang et al., 2023). It is well known that lactic acid is very abundant in solid tumors (Li et al., 2022). Tumor cells produce large amounts of lactic acid through the glycolytic pathway, leading to acidification of the tumor microenvironment (Apostolova and Pearce, 2022). The acidic state can suppress the immune system and promote tumor growth and spread. Recently, LOX was initially attempted to be used to treat tumors using lactic acid in the tumor microenvironment (Zhao et al., 2023). On the one side, LOX can break down lactic acid, reducing the acidity of the tumor microenvironment, thereby enhancing immune system function and inhibiting tumor growth and

spread (Zhao et al., 2023). On the other side, LOX catalyzes the generation of hydrogen peroxide (H_2O_2) from lactic acid, which can disrupt the redox balance within the tumor and kill tumor cells (He et al., 2021).

This paper presents the design of PPy-LOX NPs for combined PTT and EDT therapy in the treatment of breast cancer. The PPy carrier was selected based on its porous walls, hollow internal structure, excellent biocompatibility, and high photothermal efficiency. As illustrated in Scheme 1, LOX was loaded into the inner core of PPy, and PVP was coated on the surface of PPy to encapsulate the LOX and provide stabilization. LOX can oxidize lactic acid in the tumor microenvironment to form H_2O_2 , which promotes ROS generation and reduces lactic acid levels, thereby disrupting tumor microenvironment homeostasis. Exogenous NIR light irradiation significantly increased the temperature of the tumor site and further reduced 4T1 activity when combined with LOX. This work demonstrates the *in vitro* photothermal conversion ability of PPy-LOX and its scavenging ability against 4T1, providing a promising direction for future malignant tumor treatment.

2 Experimental section

2.1 Materials

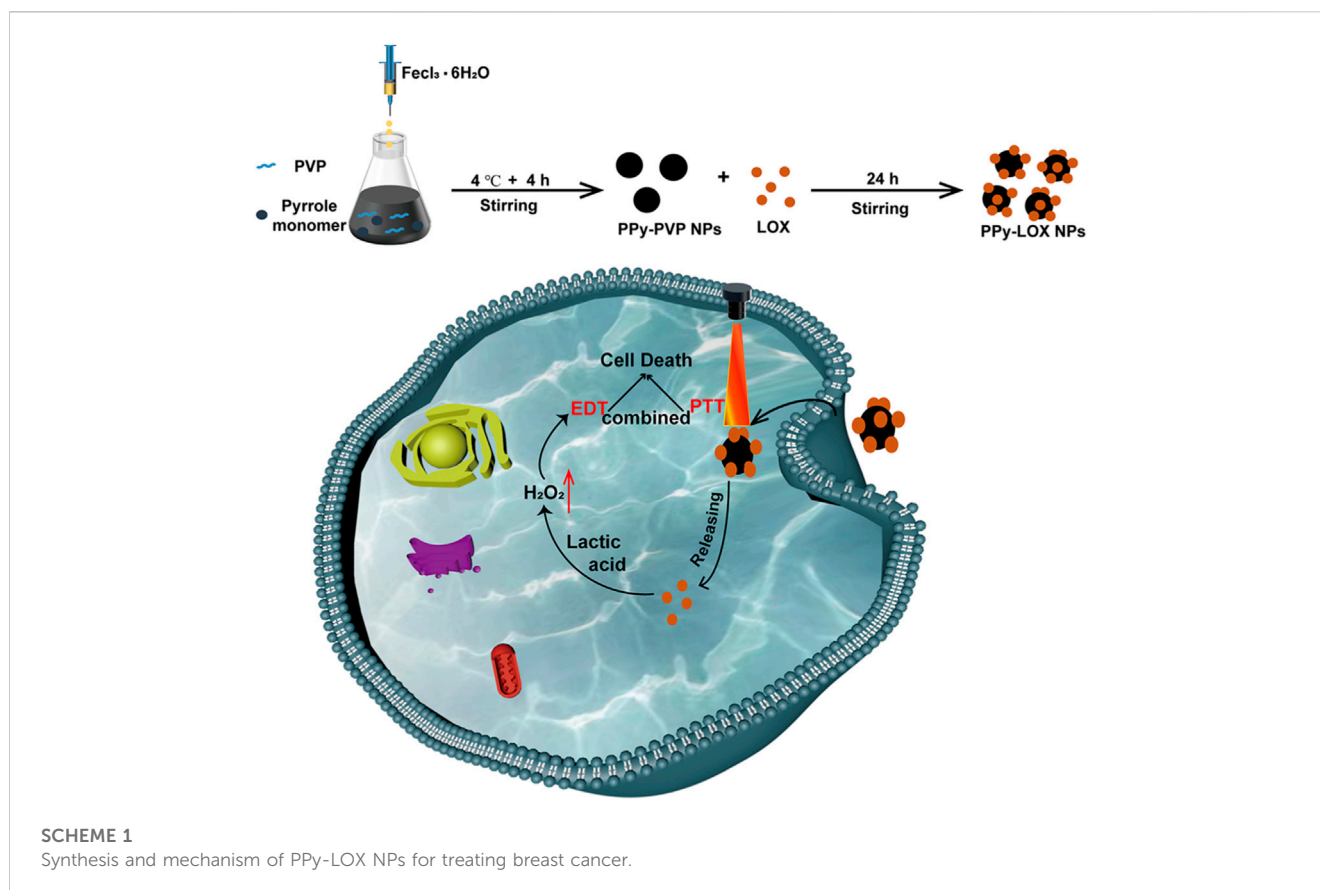
Ferric chloride hexahydrate ($FeCl_3 \cdot 6H_2O$), Pyrrole monomer, and PVP were purchased from the Aladdin Reagent Co. (Shanghai, China). Lactate Oxidase (LOX) was obtained from Sigma-Aldrich. Phosphate buffered saline (PBS), fetal bovine serum (FBS), Dulbecco's modified eagle's medium (DMEM), penicillin/streptomycin and trypsin were purchased from Gibco (United States). Cell counting kit (CCK)-8 and Enhanced BCA Protein Assay Kit were obtained from Beyotime Institute of Biotechnology. Calcein-AM/PI live cell/dead cell double staining kit was purchased from Dongren Chemical Technology (Shanghai) Co., Ltd. L929 cells and 4T1 cells were obtained from ATCC. All reagents were of analytical grade and used without further purification.

2.2 Preparation of PPy-PVP NPs

Briefly, 0.35 g of PVP (1,300 kDa) was dissolved in 80 mL of deionized water and stirred well magnetically at room temperature. Then, $FeCl_3 \cdot 6H_2O$ (3.16 g) was added and stirred well. The reaction vessel was placed in an ice-water bath and cooled to 4°C. Pyrrole monomer (200 μ L) was added and stirred for 4 h. The resulting PPy-PVP NPs were centrifuged (21,000 rpm, 15 min) and washed five times with water.

2.3 Characterization of PPy-PVP NPs

The surface morphology of the prepared PPy-PVP nanoparticles was observed using FESEM (Zeiss GeminiSEM 300, Germany). FTIR (Nicolet 7000-C spectrometer, United States) measurement was used to verify the successful preparation of PPy-PVP



nanoparticles, the data were collected with 20 scans/min by transmission mode ranging from 4000 to 400 cm^{-1} . The crystalline structure of PPy-PVP nanoparticles was studied using X-ray diffraction (XRD, Rigaku SmartLab SE, Japan) with an Angle range of 5°–90° (2 θ).

2.4 *In vitro* stability study

Dynamic light scattering (DLS) is an effective method to investigate whether PPy-LOX nanoparticles are stable under simulated physiological environment. A Zetasizer Nano series (Nano ZS 90, United Kingdom) was used to determine the changes in the particle size distribution of PPy-LOX nanoparticles with time (Day 0, 1, 3, and 5) in simulated body fluids (SBF), DMEM and Saline, respectively. The colloidal stability of PPy-LOX nanoparticles was verified by taking photographs of the Tyndall effect on days 0 and 5.

2.5 Zeta potential

To verify whether LOX was successfully loaded on the surface of PPy-PVP nanoparticles, the positive and negative electrical properties of PPy-PVP and PPy-LOX nanoparticles were tested. The Zetasizer Nano series (Nano ZS 90, United Kingdom) was used to determine the zeta potential of PPy-PVP and PPy-LOX nanoparticles, respectively.

2.6 Load efficiency of LOX

The efficiency of PPy-PVP loaded LOX was tested using the BCA assay. Different mass ratios of LOX to PPy-PVP (0.5:1, 1:1, 2:1, and 3:1) were added to deionized water and stirred at room temperature. After 24 h, the mixtures were centrifuged (9,000 rpm, 10 min). The encapsulation efficiency and loading capacity of LOX were determined using the BCA assay. The encapsulation efficiency and loading capacity were calculated using the following equation:

$$\text{encapsulation efficiency} = \frac{W - W_0}{W} \times 100\%$$

$$\text{loading capacity} = \frac{m}{m + m_1} \times 100\%$$

where W is the concentration of LOX added, W_0 is the concentration of free LOX in the suspension, m is the mass of LOX loaded in PPy-PVP and m_1 is the mass of PPy-LOX.

2.7 Enzyme activity test *in vitro*

The *in vitro* enzymatic activity of the PPy-LOX nanoparticles was verified using the methods described in previous studies. The PPy-LOX nanoparticles were fully dispersed in the lactic acid solution and the mixture was stirred in a water bath at 37°C for 30 min. Subsequently, TMB and FeCl_2 were added to the mixture and incubated in a constant temperature incubator at 37°C for

5 min. After incubation of the mixture with TMB at 37°C for 5 min, the generation of hydroxyl radical was verified by ultraviolet spectrophotometer and the color of the solution was recorded by photographing. The TMB solution treated with PPy-LOX nanoparticles + lactic acid without FeCl₂ was treated as a control. In addition, the suspension of PPy-LOX nanoparticles was placed in a dialysis bag and incubated with lactic acid solution (pH = 6.5, 37°C). The absorbance of the supernatant was measured at predetermined times to quantify H₂O₂ production.

Enzyme activity at different temperatures: Firstly, the PPy-LOX nanoparticle suspension was placed in a dialysis bag. Subsequently, the dialysis bag was placed in an EP tube containing lactic acid solution and incubated in a shaker at different temperatures (25°C–70°C) for 2 h. Finally, the lactic acid solution was collected and the lactic acid determination kit was used to quantify the lactic acid content.

2.8 *In vitro* photothermal effects of PPy

The *in vitro* photothermal effect of PPy-PVP was investigated by taking 200 µL of PPy-PVP (concentration of 50, 100, and 200 µg/mL, respectively) and placing it in a 96-well plate. The plate was then irradiated with 808 nm NIR (1 W/cm²) for 5 min, and the temperature change of PPy was recorded using an infrared thermography camera (FLIR E60, Wilsonville, OR, United States). The effect of NIR power density on PPy was investigated by taking 200 µL of PPy and placing it in a 96-well plate. The plate was then irradiated with different NIR power densities (0.6, 0.8, 1.0 W/cm²), and the temperature change of PPy-PVP was recorded using an infrared thermography camera. The photothermal stability of PPy-PVP was tested using heating and cooling curves with five “ON/OFF” cycles.

In addition, to test the photothermal conversion efficiency of PPy-PVP, we recorded the absorbance of PPy-PVP (at a concentration of 200 µg/mL) at 808 nm by UV-Vis-NIR (N4-N4s INESA). Then, PPy-PVP (at a concentration of 200 µg/mL) was irradiated with NIR (1 W/cm²) until the temperature stabilized. At this point, the irradiation was stopped and cooled naturally to room temperature, and the temperature change was recorded. The PBS was used as a control under the same conditions. The photothermal conversion efficiency of PPy was calculated using the following equation:

$$\eta = \frac{hS(T_{\max} - T_{\text{surr}}) - Q_{\text{dis}}}{I(1 - 10^{-A_{\lambda}})}$$

where *h* is the heat transfer coefficient, *S* is the surface area of the NIR-irradiated PPy-PVP, *T*_{max} is the maximum temperature of the PPy-PVP, *T*_{surr} is the room temperature at the time of the test, *I* is the NIR power, *A*_λ is the absorbance of the absorbent sample at 808 nm, and *Q*_{dis} is the heat generated by the PBS under NIR irradiation. In addition, *hS* can be obtained from the following formula:

$$hS = \frac{mC_p}{\tau_s}$$

where *m* and *C*_p are the mass and heat capacity of PBS, respectively. The *τ*_s is the time constant determined from the fitted curve of the time of PPy-PVP during the cooling process to -lnθ. The fitted curves can be calculated using the following equation:

$$t = -\tau_s \ln \left(\frac{T - T_{\text{surr}}}{T_{\max} - T_{\text{surr}}} \right)$$

where *T* is the real-time temperature of PPy-PVP at time *t*.

2.9 *In vitro* cytocompatibility

First, CCK-8 was used to detect the cytobiocompatibility of PPy-LOX. L929 cells (8 × 10³ cells/well) were inoculated in 96-well plates overnight. Afterwards, the original medium was removed and replaced with medium containing different concentrations of PPy-LOX (0, 10, 25, 50, 100 µg/mL) to continue the co-culture for 24 h. Subsequently, the co-culture medium was removed and washed twice using PBS. CCK-8 working solution was added according to the manufacturer's instructions and incubation was continued for 2 h. Absorbance at 450 nm was recorded by the zymograph to calculate the relative viability of the cells. Similarly, the Live/Dead Cell Staining Assay was used to visualize cell survival more effectively. In brief, after co-incubation with different concentrations of PPy-LOX, the original medium was replaced with calcein-AM/PI staining solution. After the plates were incubated in a dark environment for 30 min, fluorescence microscopy was used to observe the survival of the cells.

2.10 *In vitro* hemocompatibility

The hemocompatibility of PPy-LOX was evaluated by measuring the ratio of erythrocyte hemolysis. Fresh mouse anticoagulated whole blood was centrifuged (3,000 rpm, 5 min) to obtain erythrocytes, which were then washed three times with PBS to remove impurities. The collected erythrocytes were resuspended in PBS (4% w/v) and stored in a refrigerator at 4°C for backup. For hemolysis experiments, different concentrations of PPy-LOX (100, 200, 500, and 1,000 µg/mL) were added to the erythrocyte suspensions and incubated at 37°C for 2 h. The mixture was then centrifuged (3,000 rpm, 5 min), and the absorbance of the supernatant was measured at 540 nm using UV-Vis-NIR. The erythrocyte suspensions after incubation with PBS (negative control) and H₂O (positive control) were used as controls. The hemolysis ratio was calculated using the following formula:

$$\text{Hemolytic ratio (\%)} = \frac{A_n - A_b}{A_p - A_b} \times 100\%$$

Where *A*_n is the absorbance of the sample, *A*_b is the absorbance of the PBS group and *A*_p is the absorbance of the H₂O group.

2.11 *In vitro* tumor cell therapy

4T1 Cells were inoculated at a density of 8000 cells per well in 96-well plates overnight to facilitate wall attachment. Afterwards, the original medium was removed and subjected to different treatments: (a) 100 µL DMEM, (b) 100 µL DMEM (20 mM lactate), (c) 100 µL PPy-LOX (100 µg/mL) (d) 100 µL PPy (100 µg/mL) + NIR (1.0 W/cm², 5 min), (e) 50 µL PPy-LOX (200 µg/mL) + 50 µL lactate (40 mM), (f) 50 µL PPy-LOX (200 µg/mL) + 50 µL lactate (200 µg/mL) + NIR (1.0 W/cm², 5 min). After the different treatments, 4T1 cells were continued

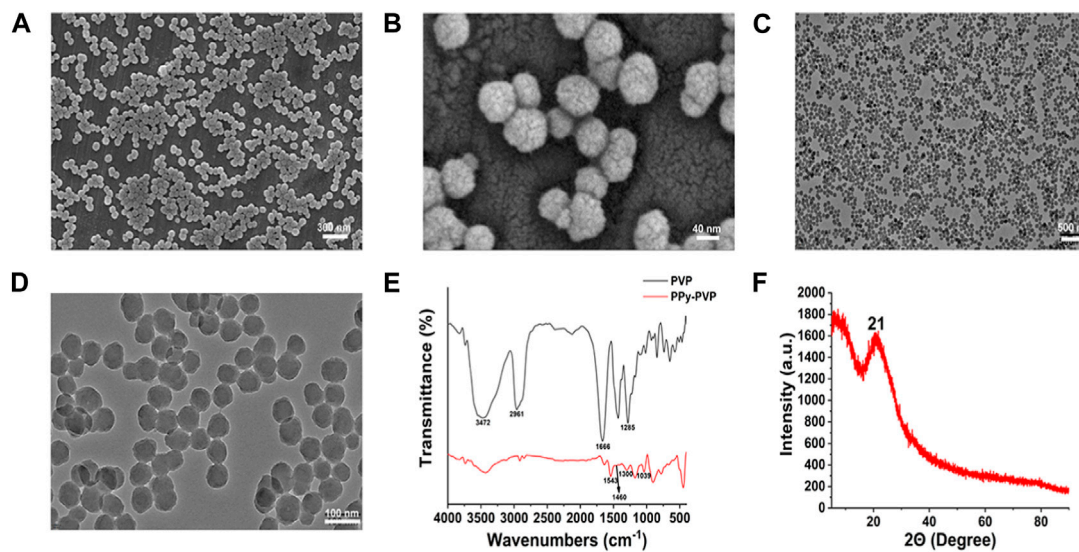


FIGURE 1

(A) FESEM image of PPY-PVP NPs. (B) Enlarged FESEM image of (A). (C, D) TEM images of PPY-PVP NPs; (E) FTIR spectra of PVP and PPY-PVP. (F) XRD pattern of PPY-PVP.

to be incubated for 24 h in the incubator. Afterwards, CCK-8 assay and Calcein-AM/PI staining were performed to examine the cell killing ability of each group, respectively. The experimental procedure is the same as in 2.8.

2.12 *In vivo* biocompatibility

All animal experiments were conducted in accordance with the Measures for Animal Management of the Ministry of Health of the People's Republic of China. 4–6 weeks old female KM mice were purchased from Slaccas Laboratory Animal Co., Ltd. (Shanghai, China). 100 μ L of saline and PPY-LOX (1,000 μ g/mL) were injected into mice through the tail vein. The KM mice were fed *ad libitum* in a quiet environment for 4 weeks, and blood was collected at predetermined time points for blood biochemical analysis. In addition, the weight changes of the mice were recorded at 4-day intervals. Finally, the major organs were collected and stained for hematoxylin-eosin (H&E) staining.

2.13 *In vivo* antitumor study

Balb/c nude (4–6 weeks, female) was chosen to evaluate the *in vivo* therapeutic effect of PPY-LOX. Briefly, the mice were subcutaneously inoculated in the right axilla with 1×10^6 4T1 cells. The tumor-bearing mice were randomly divided into 4 groups ($n = 3$). Each group was treated as follows: a. Control group (tail vein injection of 200 μ L PBS), b. PTT group ((tail vein injection of 200 μ L PPY-PVP), c. EDT group (tail vein injection of 200 μ L PPY-LOX), d. PTT/EDT group (tail vein injection of 200 μ L PPY-LOX). The control group, PTT group and PTT/EDT group were irradiated with NIR laser at the tumor site 12 h after injection (0.8 W/cm², 5 min). Tumor volume was measured every 2 days.

The tumor volume was calculated as follows: $(V) = (\text{tumor length}) \times (\text{tumor width})^2/2$. The mice were euthanized after 14 days of treatment and the weight of the tumor is recorded.

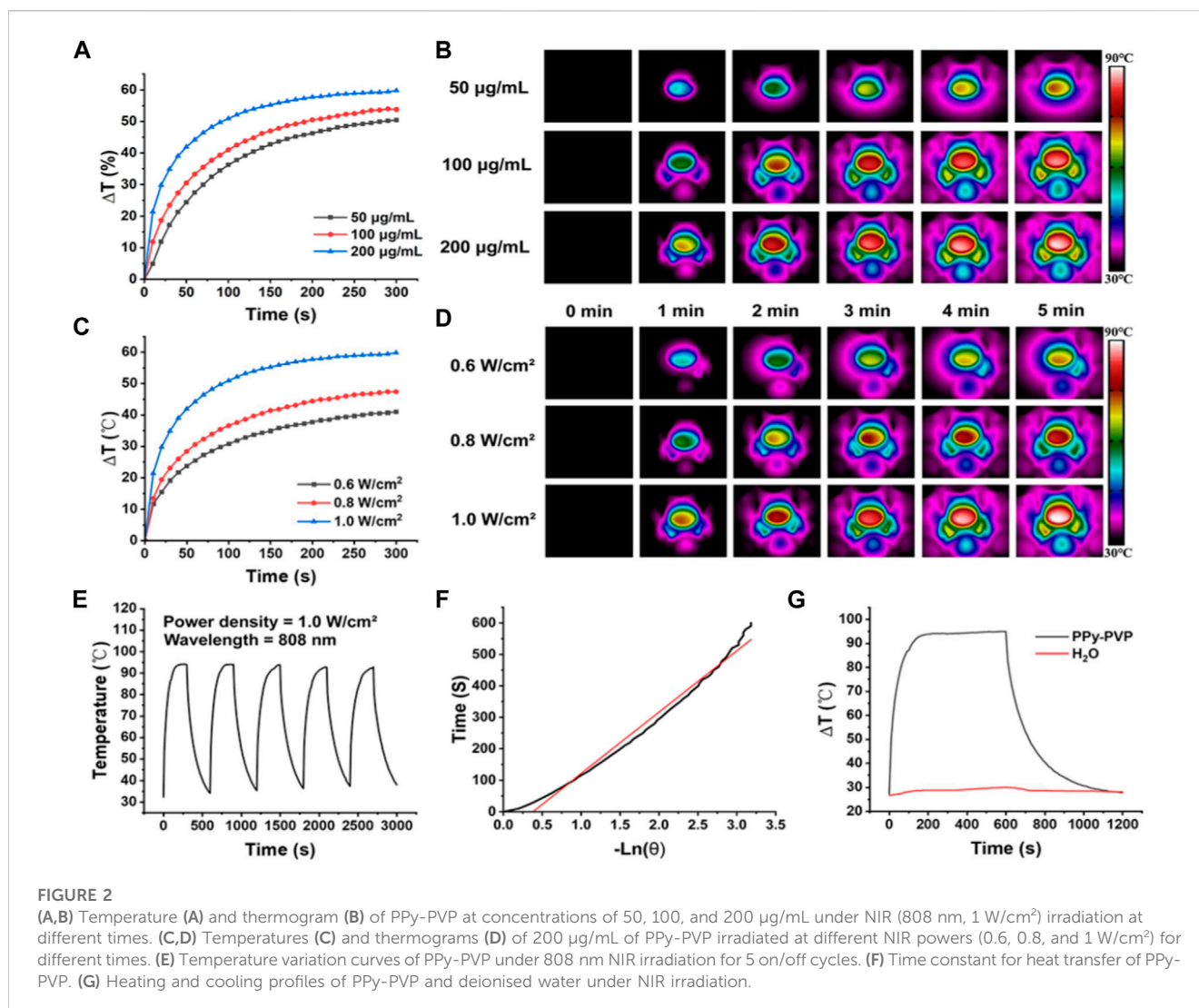
2.14 Statistical analysis

Differences were evaluated using the one-way analysis of variance (ANOVA), * $p < 0.05$, ** $p < 0.01$, *** $p < 0.001$, ns: not specified. The sample size was three ($n = 3$).

3 Results and discussions

3.1 Preparation and characterization of PPY-PVP

First, PPY-PVP NPs were synthesized and prepared using a chemical oxidation method. PVP was added as a stabilizer to modify the PPY NPs to achieve excellent colloidal stability. As a qualified carrier, it should have a special surface structure. Therefore, the microscopic morphology of PPY-PVP nanoparticles was examined by scanning electron microscopy (Figures 1A,B). It can be found that PPY-PVP nanoparticles are spheres with porous structure on the surface. This surface porous structure endows the PPY-PVP nanoparticles with excellent loading properties. Transmission electron microscopy (TEM) results showed that PPY-PVP is spherical and uniform in size (Figures 1C,D). To verify the successful modification of PVP molecules on the surface of PPY nanoparticles, FTIR measurement was used to perform structural analysis of pure PVP molecules and PPY-PVP nanoparticles (Figure 1E). From the spectrum of PPY-PVP nanoparticles, Peaks located at 1,039 cm⁻¹, 1,300 cm⁻¹, 1,460 cm⁻¹, and 1,543 cm⁻¹ could be ascribed to the characteristic C–H ring deformation, C–H in-plane bend, C–N stretching vibration and C–C conjugation of PPY nanoparticles

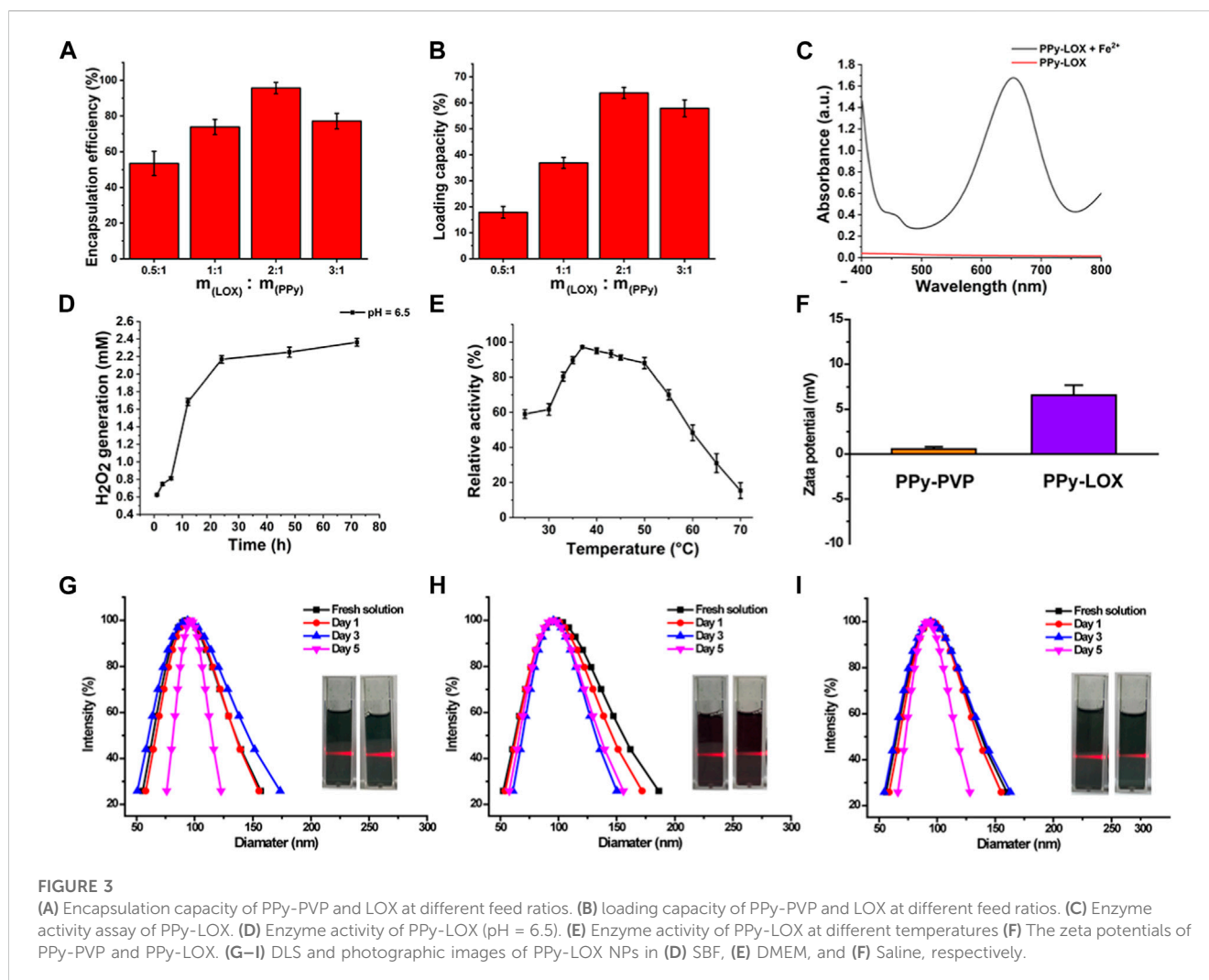


respectively. Peaks located at $2,961\text{ cm}^{-1}$, $1,666\text{ cm}^{-1}$, $1,500\text{--}1,400\text{ cm}^{-1}$, and $1,285\text{ cm}^{-1}$ corresponding to the characteristic C–H stretching/bending vibrations, C=O stretching vibration, C–N stretching vibration and $-\text{CH}_2$ deformation vibration of pure PVP molecules were detected respectively. The peak located at $3,472\text{ cm}^{-1}$ corresponded to characteristic peak of bounded water. The FTIR measurement results clearly showed that PVP molecules had been successfully modified on the surface of PPy nanoparticles. The crystal structure property of PPy-PVP nanoparticles was characterized using XRD measurement (Figure 1F). As shown in the figure, PPy correlated with a wide characteristic peak at $2\theta = 21^\circ$, clearly demonstrating the amorphous nature of PPy. The above results indicate that the successful synthesis of PPy-PVP nanoparticles.

3.2 The photothermal capacity of PPy

Previous studies have demonstrated that tumor cells undergo irreversible protein denaturation or DNA damage when exposed to temperatures exceeding 50°C . Thus, we evaluated the photothermal conversion capacity of PPy-PVP. The Figure 2A depicts the irradiation

of a $50\text{ }\mu\text{g/mL}$ PPy-PVP solution with 808 nm NIR (1 W/cm^2) when the temperature gradually stabilization and a subsequent increase of $50.4^\circ\text{C} \pm 3.1^\circ\text{C}$ after 5 min. Increasing the PPy-PVP concentration led to a further temperature increase; specifically, at a concentration of $200\text{ }\mu\text{g/mL}$, the temperature increased by $59.8^\circ\text{C} \pm 3.6^\circ\text{C}$. From the thermal images (Figure 2B) we can clearly see that there is a significant difference in the heating effect of different concentrations of PPy-PVP. In order to examine the impact of NIR power density on the photothermal capability of PPy-PVP, we exposed a solution containing $200\text{ }\mu\text{g/mL}$ PPy-PVP to NIR radiation with power densities of 0.6, 0.8, and 1.0 W/cm^2 for 5 min (Figures 2C,D). Infrared thermography indicated respective temperature increases of $41.1^\circ\text{C} \pm 2.4^\circ\text{C}$, $47.4^\circ\text{C} \pm 1.3^\circ\text{C}$, and $59.2^\circ\text{C} \pm 2.7^\circ\text{C}$ for each power density tested. These experiments confirm that adjusting both the concentration of PPy-PVP and the power of NIR irradiation can effectively control the temperature during photothermal therapy. We subsequently evaluated the photothermal stability of PPy-PVP and observed that it could maintain a maximum temperature of approximately 93°C over five “ON/OFF” cycles, indicating strong photothermal stability (Figure 2E). Photothermal conversion efficiency (η) serves as a critical metric for the assessment of photothermal converters. Utilizing information from Figures 2F,G



and [Supplementary Figure S1](#), we determined that PPy-PVP achieves a remarkable conversion efficiency of 29.9%. The photothermal conversion efficiency of PPy-PVP is comparable to numerous previously reported photothermal materials, indicating its immense potential as a photothermal therapeutic agent ([Wang et al., 2022](#); [Chen et al., 2023](#)).

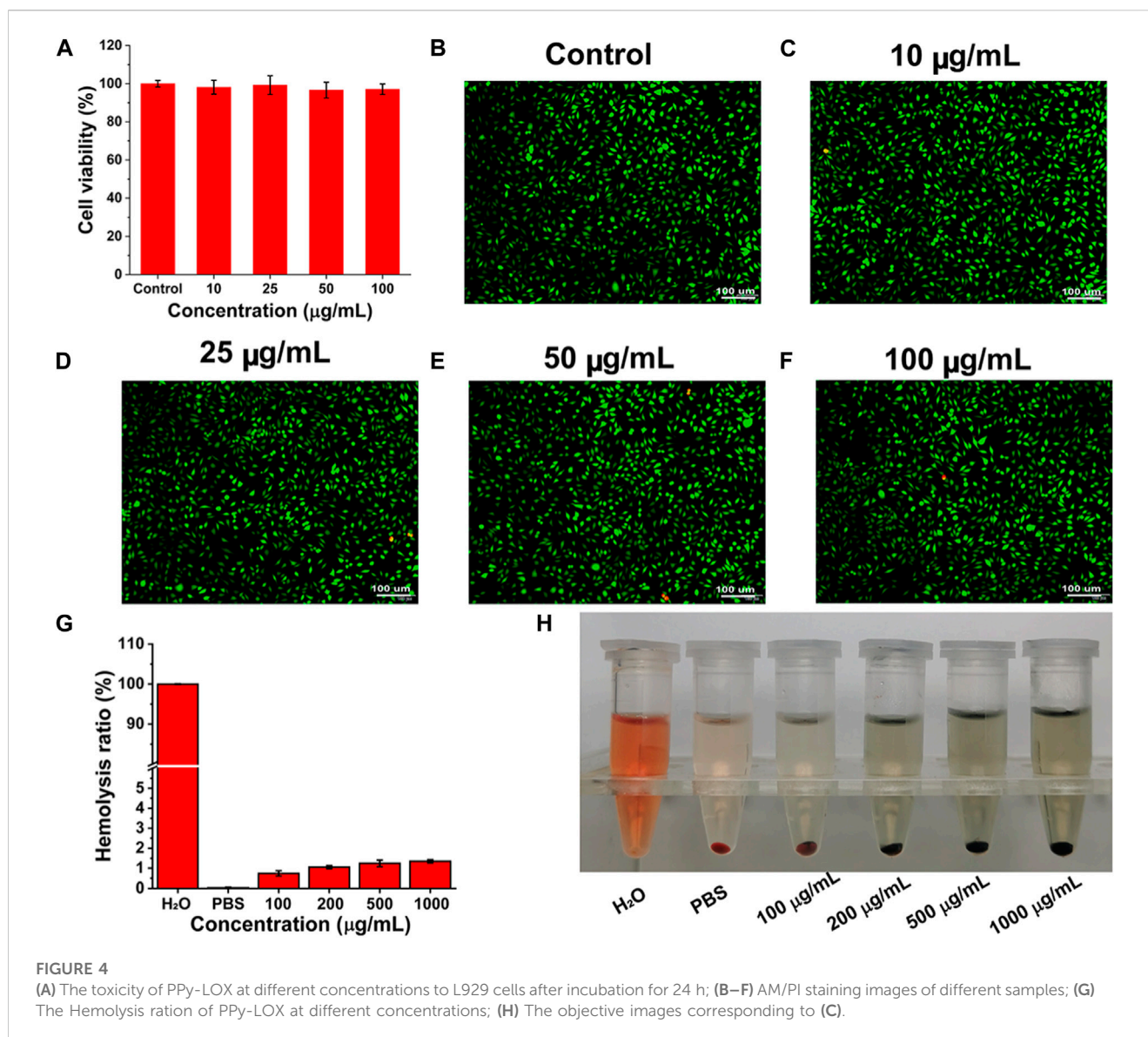
Our experiments confirmed that even at low-power NIR irradiation, low concentrations of PPy-PVP exhibit excellent photothermal conversion ability and can facilitate controllable regulation during photothermal therapy.

3.3 The loading capacity and enzyme activity of LOX

The LOX loading capacity of PPy-PVP is explored. As shown in [Figure 3A](#), when the PPy-LOX feed ratio was increased from 0.5:1 to 2:1, the LOX loading efficiency increased significantly from $53.5\% \pm 6.8\%$ to $95.7\% \pm 3.2\%$. However, as the feed ratio was increased to 3:1, the loading factor of LOX decreased slightly, indicating that the loading sites of PPy-PVP were limited. Next, the load capacity of the PPy load LOX was calculated. As shown in [Figure 3B](#), the LOX loading was as high as $63.8\% \pm 2.1\%$ at a feed ratio of 2:1. Therefore, all subsequent

experiments used a feed ratio of 2:1 parameter. To further confirm that LOX was successfully loaded, sodium dodecyl sulfate-polyacrylamide gel electrophoresis (SDS-PAGE) was performed to assess protein composition. As shown in [Supplementary Figure S2](#), the bands corresponding to the monomeric LOX (~42 kDa) could be distinctly observed in the samples of commercial LOX and PPy-LOX. TEM was used to observe the microscopic morphology of PPy-LOX, and the results showed that the loading of LOX had no visible change on the morphology of PPy-PVP ([Supplementary Figure S3](#)). The enzyme activity of LOX after loading by PPy has also been explored *in vitro* ([Figure 3C](#)). After adding FeCl_2 , the mixture solution of PPy-LOX nanoparticles + lactic acid turned blue ([Supplementary Figure S4](#)). The ultraviolet spectrophotometer detected the characteristic absorption of the mixed solution at 654 nm, clearly indicating that the enzymatic activity of LOX in the PPy-LOX nanoparticles was retained. The ability of PPy-LOX to produce H_2O_2 in a weak acidic environment is critical for the efficacy of EDT. As shown in [Figure 3D](#), the generation of H_2O_2 gradually increased with the extension of reaction time under the simulated TME conditions (pH = 6.5), proving that PPy-LOX nanoparticles retained good enzyme activity of LOX.

After loading of LOX onto the surface of PPy-PVP, the NIR absorbance feature of the PPy-LOX does not appreciably change, implying that the modification of LOX does not seem to impact the



photothermal conversion behaviors (Supplementary Figure S5). In order to investigate the feasibility of combined EDT and PTT treatment, the enzyme activity at different temperatures was studied *in vitro*. The enzyme activity of LOX in PPy-LOX nanoparticles increased at 25°C–37°C and decreased at 37°C–70°C (Figure 3E). The enzyme activity of LOX was the highest at 37°C. In the range of 37°C–45°C, the enzyme activity of LOX decreased by 6%. At 50°C, the enzyme activity of LOX decreased by about 9%. The enzyme activity of LOX decreases only slightly even up to 50°C, fully ensuring the feasibility of combining PTT and EDT for tumor treatment.

3.4 Zeta potential and dynamic light scattering

As shown in Figure 3F, the zeta potentials of PPy-PVP and PPy-LOX nanoparticles were 0.57 ± 0.25 mV and 6.57 ± 1.12 mV, respectively. PPy-PVP nanoparticles were electrically neutral, and PPy-LOX nanoparticles after loading with LOX were positively

charged. The result of the zeta potentials further indicated that the loading of LOX was successful. To improve the colloidal stability of PPy nanoparticles, PVP was used to modify their surface. PVP is a polymer that can adsorb onto the nanoparticles' surface through hydrogen bonding or van der Waals forces, forming a protective layer that prevents aggregation and precipitation in solution. The colloidal stability of PPy-LOX nanoparticles was studied using DLS. As shown in Figures 3G–I, the original hydrated particle sizes of PPy-LOX nanoparticles in SBF, DMEM and Saline were 94.07 ± 2.17 nm, 94.85 ± 4.19 nm, and 95.91 ± 1.47 nm, respectively. On day 1, the hydrated particle sizes of PPy-LOX nanoparticles in SBF, DMEM and Saline were 96.12 ± 1.78 nm, 97.36 ± 0.84 nm, and 97.28 ± 2.12 nm. On day 3, the hydrated particle sizes of PPy-PVP-LOX nanoparticles in SBF, DMEM and Saline were 96.93 ± 2.89 nm, 98.78 ± 3.01 nm, and 97.8 ± 3.19 nm, respectively. On day 5, the hydrated particle sizes of PPy-LOX nanoparticles in SBF, DMEM and Saline showed hydrated particle sizes of 99.28 ± 2.52 nm, 98.97 ± 5.04 nm, and 98.67 ± 6.75 nm, respectively. Additionally, digital photographs of the nanoparticles in each solution showed a significant Tyndall effect, indicating excellent colloidal stability.

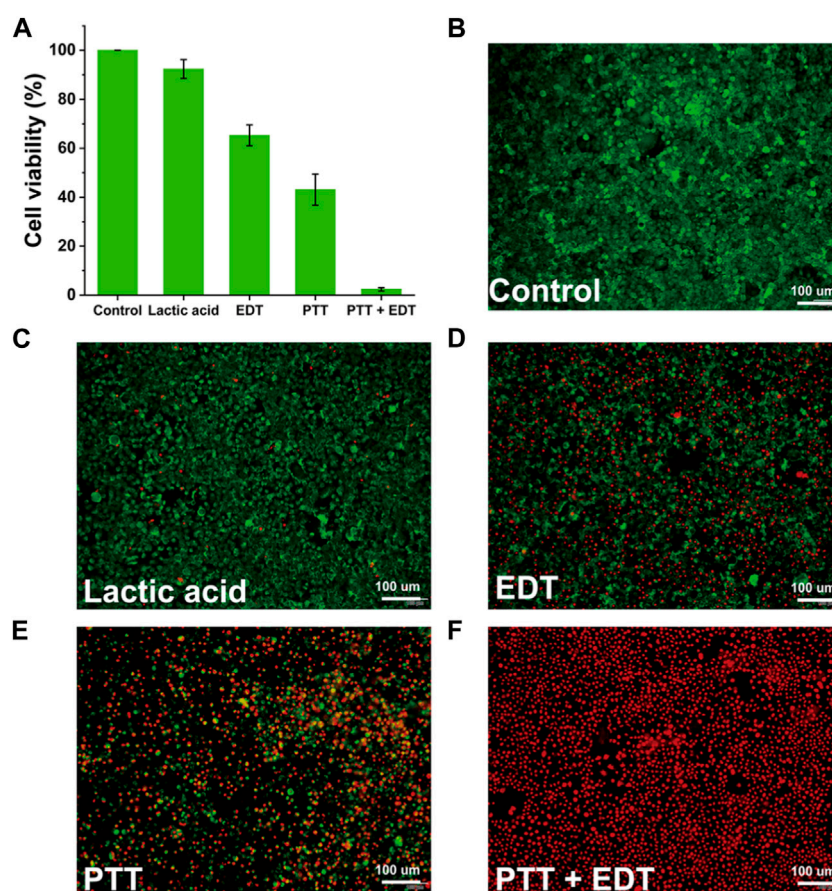


FIGURE 5

(A) Relative cell viabilities of 4T1 cells after different treatments. (B–F) Live/dead staining of 4T1 cells after different treatments.

3.5 Biocompatibility of PPy-LOX

A satisfactory anti-tumor drug should achieve its effect with minimal damage to normal cells. L929 cells were selected as a cell model to evaluate the toxicity of PPy-LOX to normal cells. As shown in Figure 4A, the results of CCK-8 showed that the survival rates of L929 cells co-incubated with different concentrations of PPy-LOX were all higher than 95% compared to the control group. Similarly, as shown in Figures 4B–F, the results of live-dead cell staining are more intuitively seen in the very small number of cells in the field of view that are colored red (dead cells). The above results showed that PPy-LOX has good biocompatibility for normal cells.

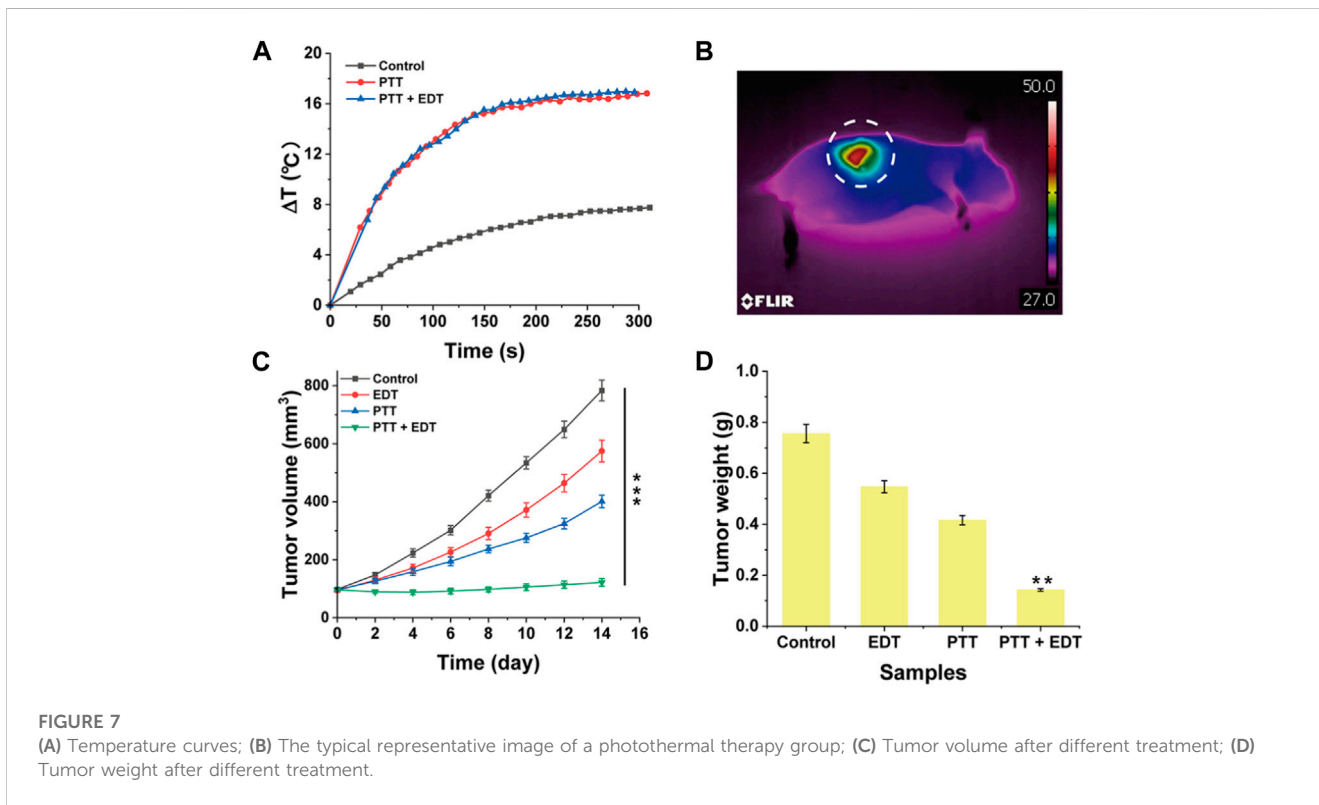
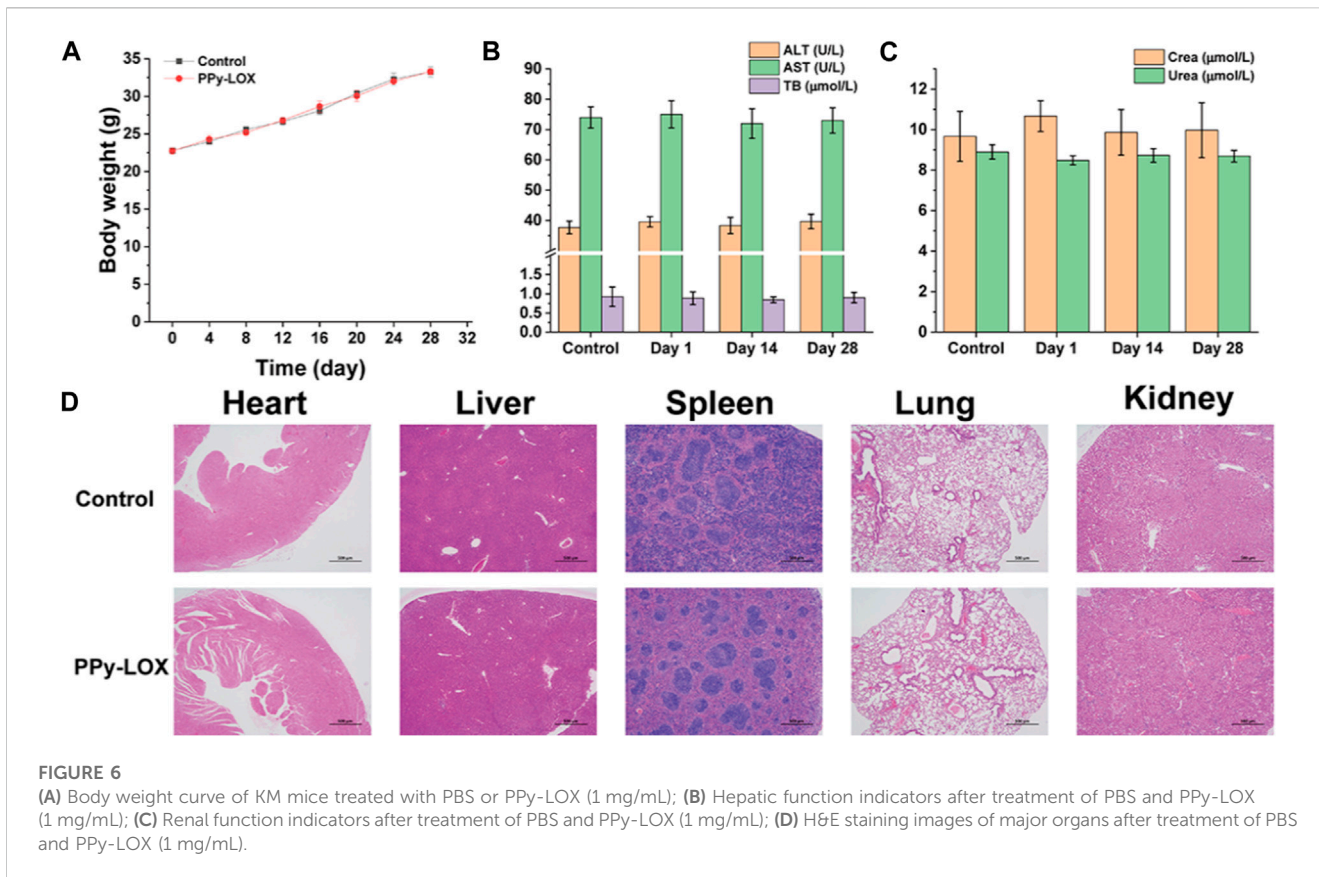
3.6 Blood safety of PPy-LOX

As intravenous injection is the primary route of administration of chemotherapeutic agents, we evaluated the hemocompatibility of PPy-LOX. As shown in Figure 4G, the ratio of hemolysis increased slightly with increasing concentration of PPy-LOX. However, even at a PPy-LOX concentration of 1,000 μg/mL, the hemolysis ratio measured in the experiment was less than 5%. Corresponding hemolysis images similarly illustrate that PPy-LOX

will not cause widespread erythrocyte rupture (Figure 4H). Therefore, PPy-LOX is safe for intravenous use due to its good hemocompatibility.

3.7 Anti-tumor efficacy in 4T1 cell model

In light of the excellent photothermal conversion properties of the synthesized PPy-LOX, the *in vitro* antitumor efficiency of PPy-LOX was next explored. As shown in Figure 5A, the viability of 4T1 cells after addition of lactic acid alone was $92.36\% \pm 3.87\%$, which was slightly decreased compared to the control group. However, after the simultaneous addition of PPy-LOX and lactic acid, cell viability decreased to $65.28\% \pm 4.28\%$. The dramatic cell death is attributed to LOX-catalyzed lactate production of highly oxidizing H_2O_2 , which kills tumor cells. Compared with no laser irradiation, the cell survival rate of 4T1 under 808 nm laser irradiation was $43.07\% \pm 6.36\%$, indicating that the high temperature induced by laser irradiation can substantially kill tumor cells. Finally, the results of the combined treatment group showed a cell survival rate of $2.35\% \pm 0.04\%$, indicating that PTT and EDT can significantly overcome the heterogeneity of tumor cells to maximize tumor cell killing. In order to visualize the anti-tumor effect more visually, live and dead cell staining was used to differentiate between live and dead cells. As shown in



Figures 5B–F, large amounts of red fluorescence were seen in both the PTT and EDT groups, but green fluorescence indicating cell survival was also present. However, the PTT + EDT group showed a full field of view with red fluorescence almost no green fluorescence was visible. The above results indicated that either PTT or EDT alone could inhibit tumor cells to some extent but could not completely overcome the heterogeneity of tumor cells. The combination of PTT and EDT can maximize the killing of tumor cells to achieve a satisfactory therapeutic effect. In addition, CCK-8 and staining results have shown that PTT and EDT have a selective killing effect with minimal side effects. Meanwhile, the concentrations of lactate and H₂O₂ in the supernatant of 4T1 cells were also examined after the treatment. As shown in Supplementary Figure S6, PPy-LOX significantly reduced the lactate concentration compared to the control group, showing a better lactate catalysing effect. The changes in H₂O₂ concentration similarly supported the ability of PPy-LOX to have the EDT treatment (Supplementary Figure S7). Nanoparticles based on conjugated polymers are now widely used in biomedical applications (Zhang et al., 2023). Compared with other studies (Li et al., 2021; Geng et al., 2023; Yu et al., 2023), we used a simple method to construct PPy-LOX nanoparticles, and the results of *in vitro* cell therapy showed that our synthesized PPy-LOX could combine PTT and EDT to kill tumor cells. We believe that the combined therapeutic strategy of PTT and EDT has great prospects for cancer nanomedicine.

3.8 *In vivo* biosafety of PPy-LOX

Encouraged by the *in vitro* therapeutic efficacy and *in vitro* biocompatibility results, in order to investigate whether PPy-LOX has potential for *in vivo* application, we performed *in vivo* biosafety experiments. As depicted in Figure 6A, after tail vein injection of PPy-LOX, the body weight of both experimental and control mice increased naturally throughout the feeding cycle without significant fluctuations. Next, blood biochemical parameters were examined to assess whether PPy-LOX affects liver and kidney function in mice. As illustrated in Figures 6B,C, compared with the control group, none of the commonly used indicators of liver and kidney function in the experimental group experienced a significant increase or decrease. The results showed that PPy-LOX injected via tail vein did not cause burden on liver and kidney functions. Finally, the major organs of both groups of mice were collected to visualize the presence of pathological damage by HE staining. As shown in Figure 6D, upon histological examination, no obvious pathological abnormalities were found in the major organs stained by H&E, further indicating that PPy-LOX nanomaterials have good biocompatibility. These experimental results confirm the biosafety of PPy-LOX nanomaterials and highlight their potential for clinical application.

3.9 *In vivo* antitumor analysis

Inspired by the excellent biocompatibility of PPy-LOX, the *in vivo* anti-tumor effect was explored. Firstly, the temperature changes at the tumor site in the photothermal therapy group were monitored. As shown in Figure 7A, The PTT and PTT + EDT groups had a temperature increase of 16.82°C and 16.91°C, respectively. However, the control group increased by only

7.76°C, suggesting that PPy-LOX can be aggregated to the tumor site through the enhanced permeability and retention effect (EPR). The thermal imaging photographs of mice more visually present the temperature changes at the tumor site under NIR irradiation (Figure 7B). Tumor volume was measured in mice every 2 days throughout the 14-day treatment cycle. The results showed that the growth of tumors was slower in the PTT and EDT groups compared to the control group, suggesting that both EDT and PTT alone inhibited tumor growth. Moreover, the PTT + EDT group exhibited almost complete inhibition of tumor growth, which fully demonstrated the feasibility of the combined application of PTT and EDT for the treatment of tumor (Figure 7C). In addition, tumor weight further confirmed the superiority of PTT/EDT combination therapy (Figure 7D). Taken together, these findings provide further evidence of the efficient antitumor effect of PPy-LOX for PTT/EDT.

4 Conclusion

Conjugated polymers such as polyacetylene, polythiophene, polyfluorene, PPy and poly (phenylene vinylidene) (PPV) have been extensively studied in biomedical fields. We used a simple chemical oxygenation method to construct PPy-PVP nanoparticles, which facilitates their mass production. Next, LOX is integrated into the overall system to minimise damage to normal tissue using TME to treat tumor. In summary, we have successfully constructed PPy-based organic photothermal agents and used them for combined PTT and EDT treatment of breast cancer. The synthesized PPy-PVP nanoparticles exhibit excellent photothermal conversion efficiency (29.9%) and high loading capacity. Furthermore, PPy-PVP loaded with LOX enables PTT and EDT combination therapy against breast cancer cells to kill most tumor cells. More importantly, both *in vivo* and *in vitro* experiments have shown that PPy-LOX has excellent biocompatibility. This work has opened a new path for the use of organic photothermal agents for combined PTT and EDT of breast cancer.

Data availability statement

The datasets presented in this study can be found in online repositories. The names of the repository/repositories and accession number(s) can be found in the article/Supplementary Material.

Ethics statement

The animal studies were approved by the Ethics Committee of Chongming Hospital, Shanghai Medical College of Health Sciences. The studies were conducted in accordance with the local legislation and institutional requirements. Written informed consent was obtained from the owners for the participation of their animals in this study.

Author contributions

MZ: Conceptualization, Data curation, Formal Analysis, Project administration, Writing—original draft. QH: Conceptualization, Data curation, Methodology, Project administration, Resources,

Writing—original draft. BZ: Supervision, Validation, Writing—review and editing. WW: Software, Supervision, Writing—review and editing.

Funding

The author(s) declare that no financial support was received for the research, authorship, and/or publication of this article.

Conflict of interest

The authors declare that the research was conducted in the absence of any commercial or financial relationships that could be construed as a potential conflict of interest.

References

- Alamdari, S. G., Amini, M., Jalilzadeh, N., Baradaran, B., Mohammadzadeh, R., Mokhtarzadeh, A., et al. (2022). Recent advances in nanoparticle-based photothermal therapy for breast cancer. *J. Control Release* 349, 269–303. doi:10.1016/j.jconrel.2022.06.050
- Apostolova, P., and Pearce, E. L. (2022). Lactic acid and lactate: revisiting the physiological roles in the tumor microenvironment. *Trends Immunol.* 43, 969–977. doi:10.1016/j.it.2022.10.005
- Barzaman, K., Karami, J., Zarei, Z., Hosseinzadeh, A., Kazemi, M. H., Moradi-Kalbolandi, S., et al. (2020). Breast cancer: biology, biomarkers, and treatments. *Int. Immunopharmacol.* 84, 106535. doi:10.1016/j.intimp.2020.106535
- Chang, X., Wu, Q., Wu, Y., Xi, X., Cao, J., Chu, H., et al. (2022). Multifunctional Au modified Ti(3)C(2)-MXene for photothermal/enzyme dynamic/immune synergistic therapy. *Nano Lett.* 22, 8321–8330. doi:10.1021/acs.nanolett.2c03260
- Chen, B., Zheng, K., Fang, S., Huang, K., Chu, C., Zhuang, J., et al. (2023). B7H3 targeting gold nanocage pH-sensitive conjugates for precise and synergistic chemo-photothermal therapy against NSCLC. *J. Nanobiotechnology* 21, 378. doi:10.1186/s12951-023-02078-9
- Davodabadi, F., Sarhadi, M., Arabpour, J., Sargazi, S., Rahdar, A., and Diez-Pascual, A. M. (2022). Breast cancer vaccines: new insights into immunomodulatory and nanotherapeutic approaches. *J. Control Release* 349, 844–875. doi:10.1016/j.jconrel.2022.07.036
- de Melo-Diogo, D., Pais-Silva, C., Dias, D. R., Moreira, A. F., and Correia, I. J. (2017). Strategies to improve cancer photothermal therapy mediated by nanomaterials. *Adv. Healthc. Mater.* 6. doi:10.1002/adhm.201700073
- Dong, B., Lim, L. M., and Hadinoto, K. (2019). Enhancing the physical stability and supersaturation generation of amorphous drug-polyelectrolyte nanoparticle complex via incorporation of crystallization inhibitor at the nanoparticle formation step: a case of HPMC versus PVP. *Eur. J. Pharm. Sci.* 138, 105035. doi:10.1016/j.ejps.2019.105035
- Fu, L. H., Wan, Y., Qi, C., He, J., Li, C., Yang, C., et al. (2021). Nanocatalytic theranostics with glutathione depletion and enhanced reactive oxygen species generation for efficient cancer therapy. *Adv. Mater.* 33, e2006892. doi:10.1002/adma.202006892
- Garcia-Martinez, L., Zhang, Y., Nakata, Y., Chan, H. L., and Morey, L. (2021). Epigenetic mechanisms in breast cancer therapy and resistance. *Nat. Commun.* 12, 1786. doi:10.1038/s41467-021-22024-3
- Geng, S., Feng, Q., Wang, C., Li, Y., Qin, J., Hou, M., et al. (2023). A versatile PDA(DOX) nanoplateform for chemo-photothermal synergistic therapy against breast cancer and attenuated doxorubicin-induced cardiotoxicity. *J. Nanobiotechnology* 21, 338. doi:10.1186/s12951-023-02072-1
- He, M., Yang, J., Qiu, K., Wu, Y., Sun, Y., and Qi, D. (2023). Super-assembly platform for diverse nanoparticles with tunable topological architectures and surface morphologies. *J. Colloid Interface Sci.* 651, 849–860. doi:10.1016/j.jcis.2023.08.020
- He, R., Zang, J., Zhao, Y., Liu, Y., Ruan, S., Zheng, X., et al. (2021). Nanofactory for metabolic and chemodynamic therapy: pro-tumor lactate trapping and anti-tumor ROS transition. *J. Nanobiotechnology* 19, 426. doi:10.1186/s12951-021-01169-9

Publisher's note

All claims expressed in this article are solely those of the authors and do not necessarily represent those of their affiliated organizations, or those of the publisher, the editors and the reviewers. Any product that may be evaluated in this article, or claim that may be made by its manufacturer, is not guaranteed or endorsed by the publisher.

Supplementary material

The Supplementary Material for this article can be found online at: <https://www.frontiersin.org/articles/10.3389/fmats.2023.1301177/full#supplementary-material>

- Hong, R., and Xu, B. (2022). Breast cancer: an up-to-date review and future perspectives. *Cancer Commun. (Lond)* 42, 913–936. doi:10.1002/cac2.12358
- Huang, X., Lu, Y., Guo, M., Du, S., and Han, N. (2021). Recent strategies for nano-based PTT combined with immunotherapy: from a biomaterial point of view. *Theranostics* 11, 7546–7569. doi:10.7150/thno.56482
- Jia, H., Truica, C. I., Wang, B., Wang, Y., Ren, X., Harvey, H. A., et al. (2017). Immunotherapy for triple-negative breast cancer: existing challenges and exciting prospects. *Drug Resist Updat* 32, 1–15. doi:10.1016/j.drug.2017.07.002
- Jiang, S., Chen, X., Lin, J., and Huang, P. (2023). Lactate-oxidase-instructed cancer diagnosis and therapy. *Adv. Mater.* 35, e2207951. doi:10.1002/adma.202207951
- Kumar, R., Raizada, P., Ahamad, T., Alshehri, S. M., Le, Q. V., Alomar, T. S., et al. (2022). Polypyrrole-based nanomaterials: a novel strategy for reducing toxic chemicals and others related to environmental sustainability applications. *Chemosphere* 303, 134993. doi:10.1016/j.chemosphere.2022.134993
- Li, B., Wang, X., Hong, S., Wang, Q., Li, L., Eltayeb, O., et al. (2021). MnO(2) nanosheets anchored with polypyrrole nanoparticles as a multifunctional platform for combined photothermal/photodynamic therapy of tumors. *Food Funct.* 12, 6334–6347. doi:10.1039/d1fo00032b
- Li, W., Yang, J., Luo, L., Jiang, M., Qin, B., Yin, H., et al. (2019). Targeting photodynamic and photothermal therapy to the endoplasmic reticulum enhances immunogenic cancer cell death. *Nat. Commun.* 10, 3349. doi:10.1038/s41467-019-11269-8
- Li, X., Yang, Y., Zhang, B., Lin, X., Fu, X., An, Y., et al. (2022b). Lactate metabolism in human health and disease. *Signal Transduct. Target Ther.* 7, 305. doi:10.1038/s41392-022-01151-3
- Li, Y., Zhang, H., Merker, Y., Chen, L., Liu, N., Leonov, S., et al. (2022a). Recent advances in therapeutic strategies for triple-negative breast cancer. *J. Hematol. Oncol.* 15, 121. doi:10.1186/s13045-022-01341-0
- Liang, Y., Zhang, H., Song, X., and Yang, Q. (2020). Metastatic heterogeneity of breast cancer: molecular mechanism and potential therapeutic targets. *Semin. Cancer Biol.* 60, 14–27. doi:10.1016/j.semcancer.2019.08.012
- Siegel, R. L., Miller, K. D., Wagle, N. S., and Jemal, A. (2023). Cancer statistics, 2023. *CA Cancer J. Clin.* 73, 17–48. doi:10.3322/caac.21763
- Soltero-Rivera, M., Groborz, S., Janeczek, M., Kormicka, J., Wierzgon, M., Arzi, B., et al. (2023). Gingiva-derived stromal cells isolated from cats affected with tooth resorption exhibit increased apoptosis, inflammation, and oxidative stress while experiencing deteriorated expansion and anti-oxidative defense. *Stem Cell. Rev. Rep.* 19, 1507–1523. doi:10.1007/s12015-023-10537-x
- Thomsen, T., and Klok, H. A. (2021). Chemical cell surface modification and analysis of nanoparticle-modified living cells. *ACS Appl. Bio Mater.* 4, 2293–2306. doi:10.1021/acsabm.0c01619
- Wang, S., Yang, Y., Wu, H., Li, J., Xie, P., Xu, F., et al. (2022). Thermosensitive and tumour microenvironment activated nanotheranostics for the chemodynamic/photothermal therapy of colorectal tumor. *J. Colloid Interface Sci.* 612, 223–234. doi:10.1016/j.jcis.2021.12.126
- Wei, H., Jiang, D., Yu, B., Ni, D., Li, M., Long, Y., et al. (2023). Nanostructured polyvinylpyrrolidone-curcumin conjugates allowed for kidney-targeted treatment of cisplatin induced acute kidney injury. *Bioact. Mater.* 19, 282–291. doi:10.1016/j.bioactmat.2022.04.006

Wu, S., Li, Y., Zhang, R., Fan, K., Ding, W., Xu, L., et al. (2021). Persistent luminescence-polypyrrole nanocomposite for dual-modal imaging and photothermal therapy of mammary cancer. *Talanta* 221, 121435. doi:10.1016/j.talanta.2020.121435

Yu, Y., Fan, P., Li, J., and Wang, S. (2023). Preparation of biocompatible manganese selenide-based nanoparticles with antioxidant and catalytic functions. *Molecules* 28, 4498. doi:10.3390/molecules28114498

Zhang, X., Zhao, J., Xie, P., and Wang, S. (2023). Biomedical applications of electrets: recent advance and future perspectives. *J. Funct. Biomater.* 14, 320. doi:10.3390/jfb14060320

Zhang, Y., Li, M., Gao, X., Chen, Y., and Liu, T. (2019). Nanotechnology in cancer diagnosis: progress, challenges and opportunities. *J. Hematol. Oncol.* 12, 137. doi:10.1186/s13045-019-0833-3

Zhao, J., Tian, Z., Zhao, S., Feng, D., Guo, Z., Wen, L., et al. (2023a). Insights into the effect of catalytic intratumoral lactate depletion on metabolic reprogramming and immune activation for antitumoral activity. *Adv. Sci. (Weinh)* 10, e2204808. doi:10.1002/advs.202204808

Zhao, S., Li, H., Liu, R., Tao, N., Deng, L., Xu, Q., et al. (2023b). Nitrogen-centered lactate oxidase nanozyme for tumor lactate modulation and microenvironment remodeling. *J. Am. Chem. Soc.* 145, 10322–10332. doi:10.1021/jacs.3c02005

Zuo, W., Fan, Z., Chen, L., Liu, J., Wan, Z., Xiao, Z., et al. (2022). Copper-based theranostic nanocatalysts for synergetic photothermal-chemodynamic therapy. *Acta Biomater.* 147, 258–269. doi:10.1016/j.actbio.2022.05.030